Journal of Hepatocellular Carcinoma

Dovepress
Taylor & Francis Group

Open Access Full Text Article

ORIGINAL RESEARCH

Intratumoral and Peritumoral Radiomics Based on DCE-MRI for Prediction of Microvascular Invasion Grading in Solitary Hepatocellular Carcinoma (≤3 cm)

Yinqiao Li*, Helin Li*, Yayuan Feng, Lun Lu, Juan Zhang, Ningyang Jia

Department of Radiology, Eastern Hepatobiliary Surgery Hospital, Third Affiliated Hospital of Naval Medical University, Shanghai, 200438, People's Republic of China

*These authors contributed equally to this work

Correspondence: Juan Zhang; Ningyang Jia, Department of Radiology, Eastern Hepatobiliary Surgery Hospital, Third Affiliated Hospital of Naval Medical University, Shanghai, 200438, People's Republic of China, Email zhangjuan0801@126.com; ningyangjia@163.com

Purpose: To explore the application value of clinical indicators, radiological features, and magnetic resonance imaging (MRI) radiomics to predict the grading of MVI in nodular hepatocellular carcinoma (≤3cm).

Methods: A total of 131 patients with hepatocellular carcinoma (HCC) and confirmed microvascular invasion (MVI) who underwent surgical resection between January 2016 and December 2022 were retrospectively analyzed. A clinical-radiological (CR) model was constructed using independent risk factors identified by logistic regression. Radiomics models based on MRI (arterial phase, portal venous phase, delayed phase) across various regions ($AVDP_{intra}$, $AVDP_{intra+peri3mm}$, $AVDP_{intra+peri5mm}$, $AVDP_{intra+peri10mm}$) were developed using the Logistic Regression (LR) classifiers. The optimal radiomics model was subsequently integrated with the CR model to construct a combined clinical-radiological-radiomics (CRR) model. Model performance was assessed using the area under the curve (AUC).

Results: Non-smooth margin and intratumoral artery were risk factors for MVI grading. The combined CRR model demonstrated the best predictive performance, with AUCs of 0.907 and 0.917 in the training and testing sets, respectively. Compared with the CR model alone, the CRR model showed a statistically significant improvement (p = 0.008, DeLong test).

Conclusion: The $AVDP_{intra+peri3mm}$ model based on MRI radiomics demonstrates good predictive performance in predicting MVI grading in HCC (≤3cm). Combining features from the CR model with those of the $AVDP_{intra+peri3mm}$ model to construct the CRR model further enhances the prediction of MVI grading.

Keywords: hepatocellular carcinoma, magnetic resonance imaging, radiomics, microvascular invasion grading

Introduction

Hepatocellular Carcinoma (HCC) poses a significant global health burden, standing as the sixth most common malignancy worldwide[1] and ranking third in cancer-related mortality globally.[2] Given its high incidence and often asymptomatic early stages, many patients are diagnosed at advanced stages, posing challenges for treatment, resulting in elevated mortality rates and poor prognosis. Despite liver resection, the 5-year recurrence rate of HCC remains as high as 50–70%.[3,4] Studies highlight the critical importance of lesions reaching or exceeding 3 cm in diameter, indicative of aggressive behavior and unfavorable prognostic outcomes.[5] Thus, there is a pressing need for early diagnosis and intervention, particularly for HCC lesions measuring ≤3 cm, to enhance overall prognosis and patient management in liver cancer.

Received: 13 February 2025
Accepted: 17 May 2025
Published: 30 May 2025

The prognosis of HCC is multifactorial, influenced by variables such as hepatitis, cirrhosis, tumor characteristics, and microvascular Invasion (MVI).[6] MVI, characterized by the infiltration of cancer cells into the vascular endothelium, notably within small branches of the portal vein in peritumoral tissue, is a well-established adverse prognostic factor in HCC, with reported incidences ranging from 15% to 57.1%.[7–9] Higher MVI grades correlate with increased rates of recurrence and shorter survival periods,[10,11] emphasizing its clinical significance. Surgical margin enlargement is often recommended in cases of MVI presence, even for small lesions, to improve patient outcomes.[12] The grading of MVI significantly impacts both surgical decision-making and clinical outcomes in HCC. Emerging evidence demonstrates that MVI-stratified surgical strategies - particularly the combination of anatomical resection with optimal margin width selection based on MVI grade can substantially improve 5-year overall survival rates while significantly reducing early recurrence.[13] However, the current diagnosis of MVI still relies on postoperative histopathological examination of resected tissues, which introduces a certain degree of delay and limits its utility in guiding surgical recommendations. These findings underscore the importance of further research into predicting MVI in HCC preoperatively, aiming to enhance patient survival rates and quality of life.

Postoperative histopathology remains the gold standard for diagnosing MVI but is subject to some degree of delay. MRI features can be used for preoperative prediction of MVI.[14] However, the subjective interpretation of MRI features and variability in MRI equipment and settings across studies contribute to discrepancies in feature evaluation, hampering MVI prediction accuracy.[15] Radiomics, a non-invasive approach, extracts high-dimensional features from images for computational analysis, markedly enhancing diagnostic precision[16] and facilitating preoperative MVI diagnosis. Due to the higher grade of MVI, the peritumoral area of HCC is rich in highly invasive cells, leading to increased recurrence rates in patients.[17] Therefore, it is recommended to expand the surgical margins. Previous studies have mainly focused on predicting the presence of MVI.[18–20] Thus, extracting radiomic features from MRI images of both intratumoral and peritumoral region to predict MVI grading is feasible.

This study aims to develop and validate a diagnostic model for preoperative MVI grading in patients with solitary HCC ≤3cm in diameter based on multi-scale radiomics of MRI, with the ultimate goal of guiding individualized surgical decision-making regarding resection margins and operative approaches.

Materials and Methods

Participants

Our study retrospectively collected data from 1756 HCC patients who underwent surgical resection at the Third Affiliated Hospital of Naval Medical University between January 2016 and December 2022. The study protocol was reviewed and approved by the Ethics Committee of the Third Affiliated Hospital of Naval Medical University. The requirement for informed consent was waived due to the retrospective design of this study. All patient identifiers were removed during data collection and analysis to ensure confidentiality and adherence to privacy protection standards. The study was conducted in compliance with the Declaration of Helsinki. Following stringent inclusion and exclusion criteria (Figure 1), 131 MVI-positive HCC patients were included. Inclusion criteria were: (a) MRI examination within two weeks before surgery, including plain, contrast-enhanced, and DWI scans; (b) curative liver resection with pathological confirmation of HCC; (c) solitary tumor with a maximum diameter ≤3cm and no distant metastatic lesions; (d) comprehensive pathological reports confirming MVI positivity. Exclusion criteria were: (a) recurrent HCC; (b) missing or unclear clinical data and MRI data; (c) previous HCC-related treatments, such as radiofrequency ablation (RF), transcatheter arterial chemoembolization (TACE), targeted therapy, radiation therapy, and immunotherapy.

Clinical and Pathological Characteristics

Demographic characteristics, including sex, age, and hepatitis status, was retrieved from the electronic medical record system. Laboratory data comprised alpha-fetoprotein, hemoglobin (HB), prothrombin time (PT), total bilirubin (TBIL), indirect bilirubin (IBIL), bile acids, albumin (ALB), pre-albumin (PA), aspartate aminotransferase (AST), alanine amino-transferase (ALT), gamma-glutamyl transferase (GGT), abnormal prothrombin, carcinoembryonic antigen, carbohydrate antigen 199 (CA199), and hepatitis B surface antigen (HBsAg). The MVI pathological report was independently reviewed

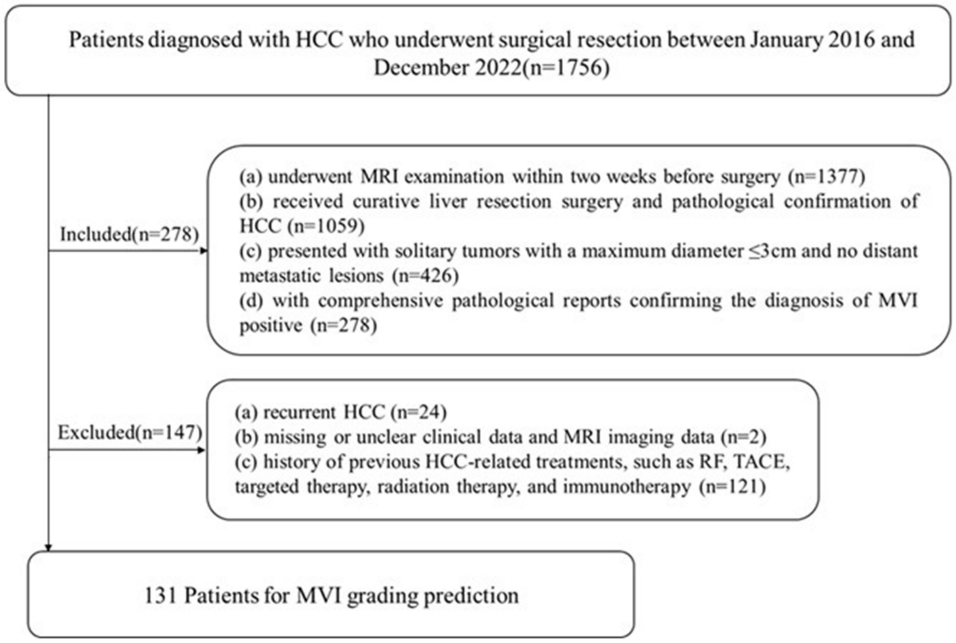

Figure 1 The workflow of patient selection for this study.

and confirmed by two proficient pathologists, each with over 10 years of experience in diagnostic pathology. MVI is defined as the presence of cancer cells nests within vessels lined by endothelial cells, commonly in the small branches of the portal vein, and less frequently in hepatic vein branches, hepatic artery, bile duct, and lymphatic vessels.[21] Pathological assessment used a 7-point baseline sampling method.[6] MVI grading is as follows:M0 indicates no MVI; M1 denotes ≤5 nests within 1cm of the tumor; M2 represents >5 nests or those located more than 1cm from the tumor.

MRI Protocol

All patients underwent MRI examinations using a 1.5T GE Signa MR scanner with an eight-channel phased-array coil, covering the entire liver. MRI sequences comprised axial T1-weighted imaging (T1WI) in-phase and out-phase, axial T2-weighted imaging (T2WI), and axial liver acquisition with volume acceleration (LAVA, GE Healthcare) dynamic contrast-enhanced imaging. Gadopentetate dimeglumine (Gd-DTPA) contrast agent was injected at 2.0 mL/s with a dose of 0.1 mmol/kg, followed by a 20 mL saline flush. The arterial phase was imaged 20–25 seconds post-contrast injection, the portal venous phase at 55–65 seconds, and the delayed phase at 120–160 seconds. Detailed scanner and scan parameters can be found in Supplementary Table 1.

Qualitative Radiographic Analysis

Two radiologists, with 8 years and 25 years of abdominal MRI experience, independently evaluated MRI features based on the Liver Imaging Reporting and Data System (LI-RADS) 2018 edition,[22] blinded to pathological results. Disagreements were resolved through consensus. The imaging features assessed included: a. Tumor maximum diameter was measured by selecting the longest length and the largest perpendicular diameter on the plane; b. Tumor margin was classified as smooth and non-smooth; c. Tumor capsule was assessed as a thin peripheral structure along the tumor margin; d. Capsule enhancement was characterized by a partial or complete peripheral rim-like enhancement around the tumor on PVP or DP; e. Peritumoral arterial phase enhancement; f. Rim enhancement; g. Washout; h. Intratumoral hemorrhage; i. Intratumoral artery; j. Intratumoral fat.

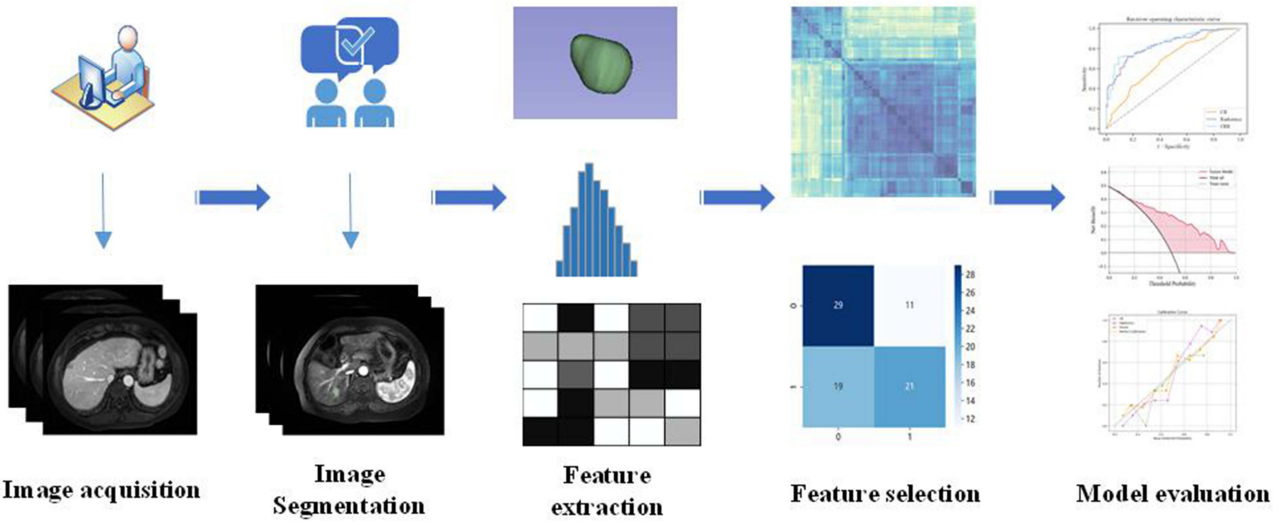

Figure 2 Flowchart of radiomics analysis.

Radiomics Analysis

The workflow of radiomics analysis, depicted in Figure 2, initiates with the extraction of patient MRI images from the Picture Archiving and Communication System (PACS) in Digital Imaging and Communications in Medicine (DICOM) format. Lesions were manually delineated on arterial, portal venous, and delayed phase MRI images by a senior radiologist utilizing 3D-Slicer software (Version 5.2.1). The delineated region was expanded by 3 mm, 5 mm, and 10 mm to create combined intratumoral and peritumoral region. Manual erasure was performed if the expanded ROI encroached upon large vessel areas surrounding the tumor or extended beyond the liver parenchyma edge. To ensure consistency, another radiologist delineated thirty cases for consistency comparison.

Subsequently, the ROI were imported into FAE software (Version 5.7) for feature extraction, yielding 1688 features: 107 features from the original images (18 first-order statistics features, 14 shape features, and 75 texture features) and 1581 high-order features from various filters (Wavelet, Square, Square Root, Logarithm, Laplacian of Gaussian, Gradient, Exponential, and Local Binary Pattern 3D). Features with an intraclass correlation coefficient (ICC) greater than 0.8 were selected and standardized using the z-score normalization. Pearson correlation coefficient was used to reduce dimensionality by merging feature pairs with a correlation coefficient ≥ 0.9. Finally, the Kruskal–Wallis test identified features associated with the MVI for model construction and evaluation.

Statistical Analysis

Statistical analyses were performed with IBM SPSS Statistics (version 26.0) and Python software (version 3.7). Independent sample *t*-tests were employed for normally distributed continuous variables, and the Mann–Whitney *U*-test for non-normally distributed data. Categorical variables were analyzed with the chi-square test or Fisher's exact test. Statistical significance was set at $p < 0.05$. Model performance was evaluated using AUC values, ROC curves, sensitivity, and specificity. Differences between models were assessed using the Delong test.

Results

Baseline Characteristics Analysis

The study included 131 patients (110 males and 21 females) with a mean age of 56.50 ± 10.46 years, of whom 97 were classified as M1 and 34 as M2. The dataset was randomly divided into a training group (n = 92) and a testing group (n = 39) at a ratio of 7:3. Statistical comparisons between the training and testing group showed no significant differences in clinical parameters ($p > 0.05$), detailed characteristics analysis can be found in Table 1

Table 1 Baseline Characteristics of HCC Patients with MVI Positive

Variable	Total (n=131)	Train (n=92)	Test (n=39)	P Value
Clinical features				
Age(years)	56.50 ± 10.46	55.1 ± 10.55	58.85 ± 9.97	0.095
Gender (n, %)				0.193
Male	110 (84.00)	80 (87.00)	30 (76.9)	
Female	21 (16.00)	12 (13.00)	9 (23.1)	
Hepatitis				0.178
None	9 (6.90)	4 (4.30)	5 (12.80)	
HBV	121 (92.40)	87 (94.60)	34 (87.20)	
HCV	1 (0.80)	1 (1.10)	0 (0.00)	
AFP(μg/L)				0.326
≤20	50 (38.2)	38 (41.30)	12 (30.80)	
>20	81 (61.8)	54 (58.70)	27 (69.20)	
HB(g/L)	139.15 ± 15.98	140.52 ± 15.32	135.92 ± 17.20	0.133
TBIL(μmol/L)	15.72 ± 8.90	14.98 ± 7.78	17.47 ± 10.99	0.144
Alb(g/L)	42.63 ± 5.55	42.55 ± 4.38	42.81 ± 7.72	0.805
PA(g/L)	209.63 ± 49.68	212.30 ± 45.62	203.33 ± 52.39	0.347
PT(s)	11.88 ± 1.08	11.87 ± 0.93	11.91 ± 1.40	0.860
IBIL(μmol/L)	9.74 ± 5.41	9.31 ± 4.94	10.74 ± 6.61	0.169
ALT(U/L)	31.33 ± 22.00	30.89 ± 23.30	32.36 ± 18.85	0.729
AST(U/L)	31.32 ± 17.78	31.52 ± 18.83	30.85 ± 15.26	0.847
GGT(U/L)	54.07 ± 56.39	51.73 ± 58.27	59.59 ± 51.99	0.468
PIVK-II (mAU/mL)				0.208
≤40	38 (29.00)	30 (32.60)	8 (20.50)	
>40	93 (71.00)	62 (67.40)	31 (79.50)	
Tba(μmol/L)	13.18 ± 18.57	12.42 ± 17.62	14.97 ± 20.77	0.475
HBsAg				0.142
Negative	15 (11.50)	8 (8.70)	7 (17.90)	
Positive	116 (88.50)	84 (91.30)	32 (82.10)	
CEA	2.52 ± 1.38	2.49 ± 1.40	2.58 ± 1.36	0.724
CA199				0.123
<30	109 (83.20)	80 (87.00)	29 (74.40)	
>30	22 (16.80)	12 (13.00)	10 (25.60)	
HBV-DNA				0.171
<50	80 (61.10)	60 (65.20)	20 (51.30)	
>50	51 (38.90)	32 (34.80)	19 (48.70)	
MRI features				
Tumor size	1.99 ± 0.56	2.01 ± 0.56	1.94 ± 0.57	0.352
Tumor margin				0.332
Smooth	54 (41.20)	35 (38.00)	19 (48.70)	
Non-smooth	77 (58.80)	57 (62.00)	20 (51.30)	
Tumor capsule				0.768
Complete	15 (11.50)	10 (10.90)	5 (12.80)	
Incomplete	116 (88.50)	82 (89.10)	34 (87.20)	
Capsule enhancement				0.169
Absence	18 (13.70)	10 (10.90)	8 (20.50)	
Presence	113 (86.30)	82 (89.10)	31 (79.50)	
Arterial peritumoral enhancement				0.229
Absence	60 (45.80)	39 (42.40)	21 (53.80)	
Presence	71 (54.20)	53 (57.60)	18 (46.20)	

(*Continued*)

Table 1 (Continued).

Variable	Total (n=131)	Train (n=92)	Test (n=39)	P Value
Rim enhancement				0.436
Absence	50 (38.20)	33 (35.90)	17 (43.60)	
Presence	81 (61.80)	59 (64.10)	22 (56.40)	
Wash out				0.651
Absence	40 (30.50)	27 (29.30)	13 (33.30)	
Presence	91 (69.50)	65 (70.70)	26 (66.70)	
Intratumoral hemorrhage				0.832
Absence	127 (96.90)	89 (96.70)	38 (97.40)	
Presence	4 (3.10)	3 (3.30)	1 (2.60)	
Intratumoral artery				0.518
Absence	56 (42.70)	41 (44.60)	15 (38.50)	
Presence	75 (57.30)	51 (55.40)	24 (61.50)	
Intratumoral fat				0.339
Absence	67 (51.10)	50 (54.30)	17 (43.60)	
Presence	64 (48.90)	42 (45.70)	22 (56.40)	

Abbreviations: AFP, alpha-fetoprotein; HB, hemoglobin; PT, prothrombin time; TBIL, total bilirubin; IBIL, indirect bilirubin, Tba, bile acids; ALB, albumin; PA, pre-albumin; AST, aspartate aminotransferase; ALT, alanine aminotransferase; GGT, gamma-glutamyl transferase; PIVKII, protein Induced by vitamin K absence or antagonist-II; CEA, carcinoembryonic antigen; CA199, carbohydrate antigen 199; HBsAg, hepatitis B surface antigen; HBV, hepatitis B virus.

Performance of CR Model

Univariate analysis identified two features significantly associations with MVI grading: non-smooth margin (OR 6.222, 95% CI: 1.696, 22.833, p=0.006) and intratumoral artery (OR 3.182, 95% CI: 1.126, 8.994, p=0.029), as shown in Table 2. These associations were observed at a significance level of $p < 0.05$. These features were used to develop the predictive CR model for MVI grading, achieving an AUC of 0.744 in the training set and 0.590 in the test set, respectively.

Performance of Radiomics Model

In the training group, the AUC values for single sequences were similar, but the $AVDP_{intra+peri3mm}$ model notably enhanced predictive performance. However, $AVDP_{intra+peri5mm}$ model and $AVDP_{intra+peri10mm}$ model led to decreased performance (Figure 3). Compared to the other models, the $AVDP_{intra+peri3mm}$ model achieved the most favorable predictive performance (Figure 4).

Table 2 Clinical and Radiological Features for Predicting Microvascular Invasion Grading

Variable	Univariate		Multivariate	
	OR	P Value	OR	P Value
Age	0.600 (0.231,1.557)	0.294		
Gender (Male vs Female)	0.527 (0.107,2.600)	0.432		
HBV (presence vs absence)	1.437 (0.15,13.537)	0.751		
HB, g/L(≤150 vs >150)	1.389 (0.508,3.795)	0.522		
TBIL,μmol/L(≤23 vs >23)	0.792 (0.153,4.106)	0.781		
Alb(≤40 vs >40)	2.714 (0.725,10.167)	0.138		
PA(≤200 vs >200)	1.636 (0.573,4.673)	0.358		
PT,s(≤13 vs >13)	0.448 (0.158,1.270)	0.131		

(*Continued*)

Table 2 (Continued).

Variable	Univariate		Multivariate	
	OR	P Value	OR	P Value
AFP,μg/L(≤20 vs >20)	0.980 (0.381,2.520)	0.967		
IBIL,μmol/L(≤15 vs >15)	0.792 (0.153,4.106)	0.781		
ALT,U/L(≤40 vs >40)	2.115 (0.746,5.996)	0.159		
AST,U/L(≤35 vs >35)	1.083 (0.368,3.192)	0.885		
GGT,U/L(≤45 vs >45)	0.978 (0.365,2.623)	0.965		
PIVK-II, (≤40 vs >40)	0.957 (0.356,2.572)	0.930		
Tba (≤12 vs >12)	0.789 (0.256,2.438)	0.681		
HBsAg (negative vs positive)	2.639 (0.308,22.646)	0.376		
CEA, μg/L (<10 vs ≥10)	0.550 (0.182,1.667)	0.291		
CA199,U/mL (<39 vs ≥39)	0.168 (0.021,1.351)	0.094		
HBV-DNA,IU/mL (<50 vs ≥50)	0.917 (0.343,2.451)	0.862		
Tumor size	1.350 (0.560,3.253)	0.504		
Tumor margin (smooth vs unsmooth)	6.222 (1.696,22.833)	**0.006**	6.442 (0.775,53.566)	0.085
Tumor capsule (complete vs incomplete)	0.803 (0.190,3.392)	0.766		
Capsule enhancement (presence vs absence)	0.484 (0.124,1.889)	0.296		
Arterial peritumoral enhancement (presence vs absence)	0.961 (0.374,2.467)	0.933		
Rim enhancement (presence vs absence)	2.660 (0.888,7.968)	0.081		
Wash out (presence vs absence)	0.746 (0.259,2.148)	0.587		
Intratumoral hemorrhage (presence vs absence)	0.164 (0.014,1.899)	0.148		
Intratumoral artery (presence vs absence)	3.182 (1.126,8.994)	**0.029**	2.364 (0.861,6.493)	0.085
Intratumoral fat (presence vs absence)	0.990 (0.389,2.520)	0.983		

Notes: Bold text indicates statistically significant results (P < 0.05).

Abbreviations: AFP, alpha-fetoprotein; HB, hemoglobin; PT, prothrombin time; TBIL, total bilirubin; IBIL, indirect bilirubin, Tba, bile acids; ALB, albumin; PA, pre-albumin; AST, aspartate aminotransferase; ALT, alanine aminotransferase; GGT, gamma-glutamyl transferase; PIVK-II, protein Induced by vitamin K absence or antagonist-II; CEA, carcinoembryonic antigen; CA199, carbohydrate antigen 199; HBsAg, hepatitis B surface antigen; HBV, hepatitis B virus.

In the test group, the AUC value trends mirrored those of the training set but were slightly lower. Nevertheless, combining intratumoral and peritumoral features across multiple phases improved AUC values. The Delong test showed no significant difference between classifiers (P > 0.05). Comprehensive evaluation of AUC values, decision curve analysis (DCA) curves, and calibration curves, identified the $AVDP_{intra+peri3mm}$ model as optimal, with an AUC of 0.863 (95% CI: 0.778–0.949) in the training group and 0.700 (95% CI: 0.515–0.868) in the test group. Detailed values for each radiomics model can be found in Supplementary Table 2.

Performance of CRR Model and Model Comparison

Combination the 2 CR model features (non-smooth tumor margin, intratumoral artery) with the 10 radiomics features of $AVDP_{intra+peri3mm}$ constructed the CRR model. The CRR model achieved an AUC of 0.917 (95% CI: 0.856–0.970) significantly outperforming both the CR model (AUC: 0.741) and the $AVDP_{intra+peri3mm}$ model (AUC: 0.863). Furthermore, the sensitivity of the CRR model (91.2%) surpassed that of the CR model (66.3%) and the $AVDP_{intra+peri3mm}$ model (30.0%) (Table 3). Delong test analysis revealed no significant difference between the $AVDP_{intra+peri3mm}$ model and the CRR model (Table 4), although the CRR model exhibited significantly improved predictive performance compared to the CR model (p=0.008). Combined decision curve and calibration curve analyses (Figure 5) underscored the superior predictive performance of the CRR model.

Discussion

MVI plays a pivotal role in determining the aggressiveness of HCC, significantly impacting both intrahepatic and distant metastases,[21] with an incidence rate ranging from 18.1% to 40.6% in hepatocellular carcinoma (≤3cm).[23–27] Notably,

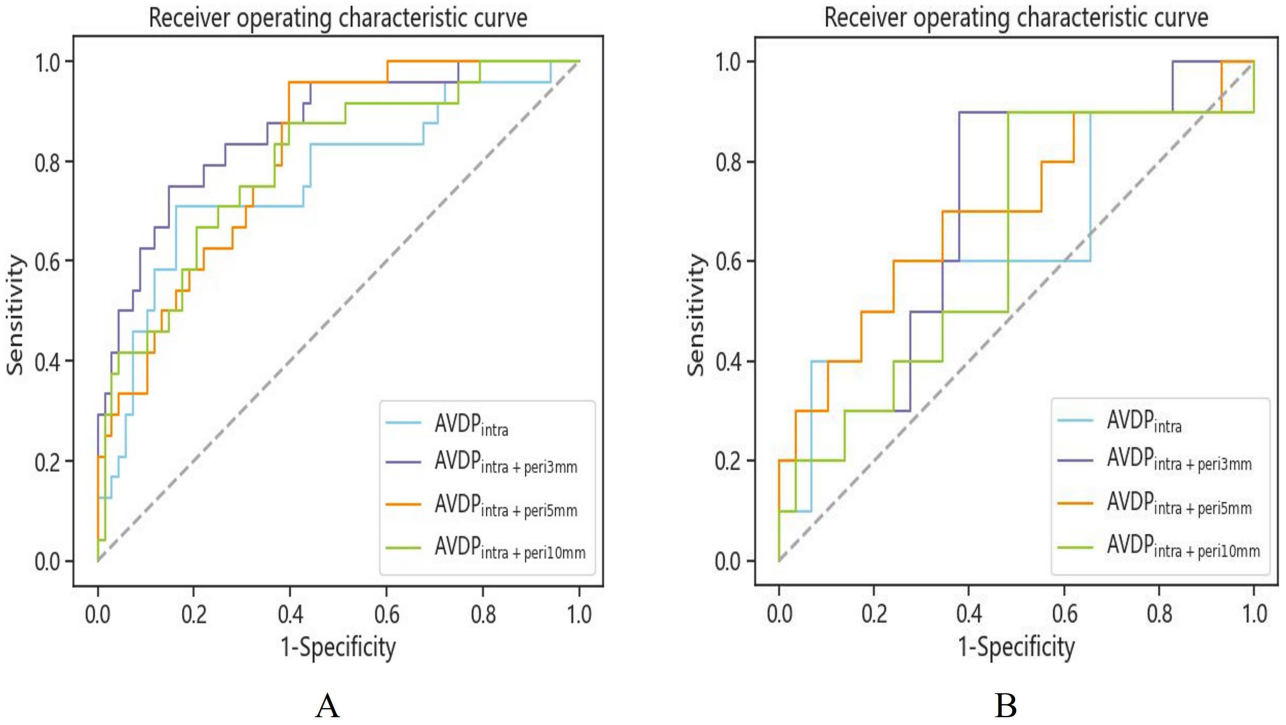

Figure 3 ROC curve of radiomics model (**A**) triphasic model in the training group, (**B**) triphasic model in the testing group.

HCC lesions smaller than 3cm are generally associated with lower invasiveness and a more favorable prognosis.[28] Consequently, patients with such tumors often opt for radiofrequency ablation therapy. However, emerging evidence suggests that among patients with HCC diameter <3cm, those harboring MVI-positive tumors undergoing radiofrequency ablation exhibit shorter overall survival and a higher frequency of local recurrence compared to MVI-negative counterparts.[23] This underscores the critical role of MVI grading in prognostication. Indeed, Lauwers et al[29] demonstrated through univariate analysis that 51% of cases exhibited MVI, with multivariate analysis revealing MVI grading, similar to tumor grading, as an independent predictor of poor survival outcomes. Significantly, the 3-year recurrence rates were markedly higher for M2 patients (86.1%) in comparison to M1 patients (71.6%). Against this backdrop, our study sought to address the imperative need for robust predictive models to stratify MVI grading in HCC ≤3cm in diameter. Our findings underscore the significance of certain MRI-based radiomics features, particularly non-smooth tumor margin and intratumoral artery, in predicting MVI grading. These features, predominantly extracted from triphasic phase imaging combined with a 3mm expansion, yielded promising discriminatory performance.

In preoperative assessment, certain MRI features can indicate the risk of MVI in patients with HCC. A recent meta-analysis[30] demonstrated a significant correlation between multiple MRI features and MVI, including tumor size, rim enhancement, arterial peritumoral enhancement, peritumoral hypointensity on HBP, non-smooth tumor margin, and multifocality. Arterial peritumoral hyperenhancement and peritumoral hypointensity on HBP are associated with MVI, possibly due to changes in peritumoral perfusion.[8] Furthermore, YANG et al[31] found that tumor size, capsule, margin, and peritumoral arterial enhancement features are associated with MVI. They also observed a significant statistical difference in intratumoral artery between the MVI-positive and negative groups, although further research on MVI grading was not conducted. In contrast, our study focused on the predictive utility of MRI features, specifically non-smooth tumor margin and intratumoral artery, in determining MVI grading. The non-smooth tumor margin, indicative of the aggressive biological behavior of HCC, emerged as a critical preoperative indicator of MVI, closely correlated with MVI grading. Through univariate and multivariate analyses, we found that intratumoral artery were more frequently observed in the M2 group compared to the M1 group. This may suggest an increased association between vascularization and higher MVI grading.

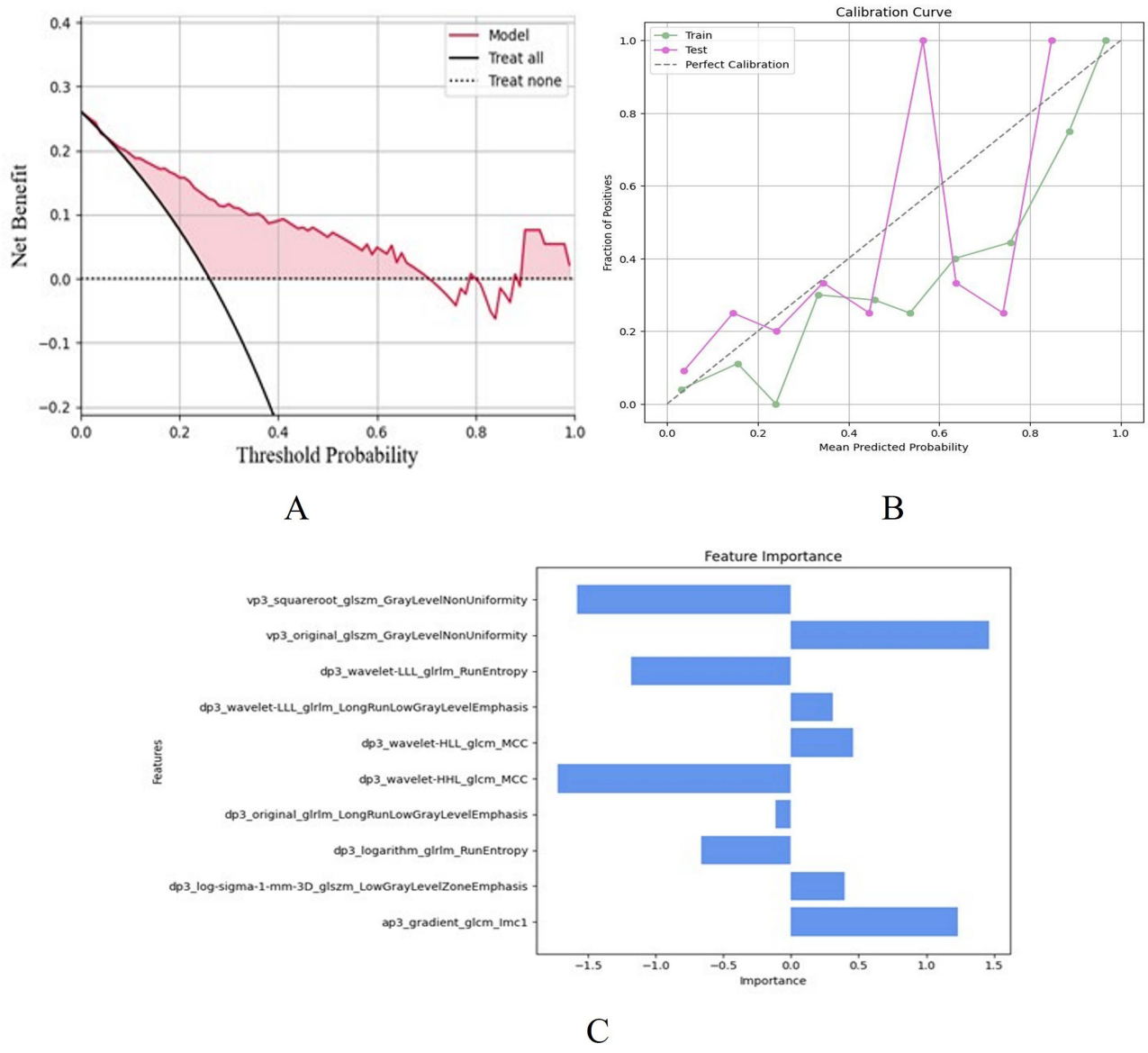

Figure 4 Performance of $AVDP_{intra+peri3mm}$ model (**A**) DCA curve of $AVDP_{intra+peri3mm}$ model, (**B**) Calibration curve of $AVDP_{intra+peri3mm}$ model, (**C**) the feature importance of $AVDP_{intra+peri3mm}$ model.

The recent study[32] established a three-class classification model based on CT images for predicting MVI grading. Similarly, our $AVDP_{intra+peri3mm}$ model, incorporating radiomics features from the AP, PVP and DP, exhibited slightly superior performance compared to the M1 model (AUC: 0.764 vs 0.680). This could be attributed to the superior clarity

Table 3 Performance Comparison of Predictive Models

Model	AUC		ACC	Spe	Sen
	Train	Test			
CR	0.744(0.633–0.856)	0.590(0.519–0.674)	0.739	0.333	0.663
$AVDP_{intra+peri3mm}$	0.863(0.778–0.965)	0.700(0.515–0.885)	0.641	0.759	0.300
CRR	0.907(0.803–0.992)	0.917(0.826–0.999)	0.859	0.667	0.912

Abbreviations: AUC, area under curve; ACC, accuracy; Spe, specificity; Sen, sensitivity.

https://doi.org/10.2147/JHC.S519578

Table 4 Delong Test of CR Model, $AVDP_{intra+peri3mm}$ Model, and CRR Model

Model	P Value
CR vs $AVDP_{intra+peri3mm}$	0.087
CR vs CRR	**0.008**
$AVDP_{intra+peri3mm}$ vs CRR	0.302

Note: Bold text indicates statistically significant results (P < 0.05).
Abbreviation: CR, clinical-radiological model.

of MRI images compared to CT images, as well as the increased stability of binary classification models over three-class classification models, resulting in more reliable predictions. The presence of MVI within 1 cm of the tumor margin is well-documented,[21] often indicating tumor heterogeneity and the presence of highly invasive cells, which significantly

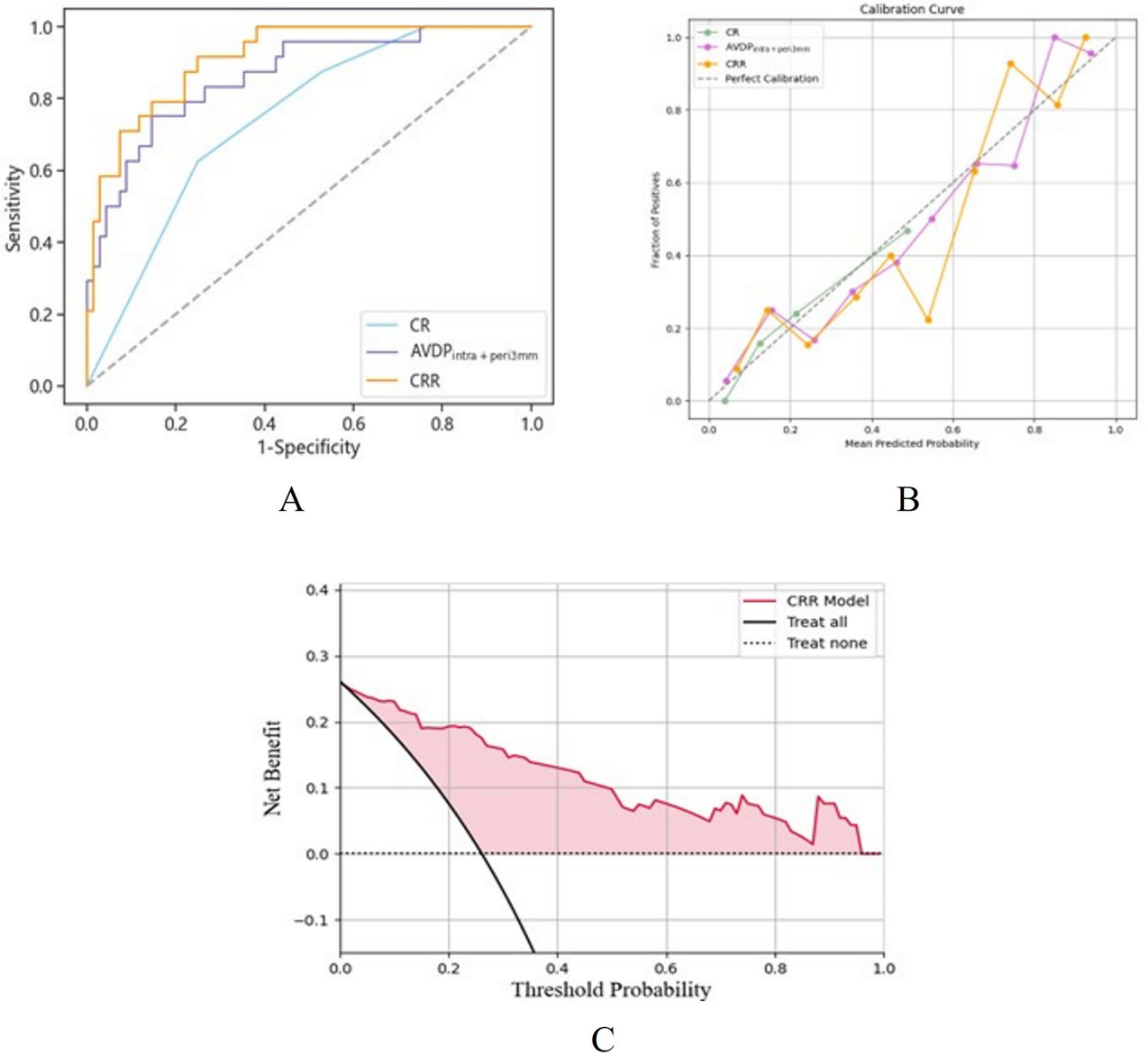

Figure 5 Performance of the CRR models (**A**) ROC curve of CR model, $AVDP_{intra+peri3mm}$ model and CRR model, (**B**) Calibration curve of CR model, $AVDP_{intra+peri3mm}$ model and CRR model, (**C**) DCA curve of CRR model.

impact liver cancer metastasis, postoperative recurrence, and prognosis.[33] Therefore, for patients with high-grade MVI, expanding the surgical margin is recommended to improve overall survival and recurrence-free survival.[34] Previous investigations[35,36] have explored the prediction of MVI by applying ROI expansion towards the tumor periphery, highlighting the effectiveness of models incorporating features extracted from both intratumoral and peritumoral region. However, the lack of a standardized measure for the extent of expansion remains a challenge. Hence, our study aimed to determine the optimal surgical resection margin for MVI grading by employing ROI expansion methods, including expansions of 3mm, 5mm, and 10mm towards the tumor periphery during ROI delineation. Single-sequence and multi-sequence MRI radiomics models were established for intratumoral and peritumoral region. Our findings demonstrated that the $AVDP_{intra+peri3mm}$ model generally outperformed the intratumoral model (AUC: 0.863 vs 0.764), as well as the 5mm and 10mm intratumoral and peritumoral models (AUC: 0.810, 0.794).

Among the features of radiomic models, there are indicators reflecting tumor homogeneity, with higher values indicating greater tumor heterogeneity, such as glszm_GrayLevelNonUniformity, glszm_GrayLevelNonUniformityNormalized, and glszm_SizeZoneNonUniformity. This result is consistent with previous research,[37] indicating that as the grade of MVI increases, tumor heterogeneity also rises, leading to poorer intratumoral grayscale uniformity and increased mixed signals. Tumor heterogeneity is primarily manifested through variations in tumor cell density, necrosis, and inflammation. The inflammatory microenvironment may contribute to the occurrence and progression of MVI,[37] and neutrophils play a crucial role in maintaining the tumor microenvironment by exerting pro-cancer effects and enhancing tumor cell invasion, metastasis, angiogenesis, and extracellular matrix remodeling.[38] Proinflammatory cytokines can activate transcription factors such as NF-κB and STAT3, thereby regulating tumor angiogenesis and invasiveness.[39] As the grade of MVI increases, tumor heterogeneity also increases, resulting in poorer intratumoral grayscale uniformity and increased mixed signals. In the final stage of our study, our study employed a method that combines clinical-radiological (CR) models with $AVDP_{intra+peri3mm}$ radiomic features to construct a CRR model for predicting MVI grading in HCC≤3cm. The results demonstrated that the predictive performance of the CRR model was comparable to that of the combined model proposed by FENG et al,[37] which was based on Gd-EOB-DTPA-enhanced MRI, and the MVI grading prediction model developed by ZHENG et al.[32] Given the robust performance of the CRR model and its ability to capture tumor heterogeneity associated with MVI grade, the findings of our study have important implications for clinical practice. In particular, for patients predicted to have high-grade MVI, wider surgical resection margins—specifically 3 cm—may be recommended to reduce the risk of residual microscopic disease, improve recurrence-free survival, and ultimately enhance long-term outcomes. Additionally, these patients may benefit from more intensive postoperative surveillance protocols. Our results thus support the potential of the CRR model to guide individualized surgical planning in early-stage HCC (≤3 cm).

This study still has some limitations. Firstly, it is a retrospective study, which may introduce selection bias. Secondly, as this study is based on retrospective analysis of samples from 2016 to 2022, Gd-EOB-DPTA were not used for hepatobiliary phase scanning during MRI scans in the past, leading to a lack of in-depth investigation into hepatobiliary phase radiomics features. Thirdly, due to the inclusion of patients with HCC≤3cm, there were relatively few cases of M2 grading. Fourthly, some cases included in this study are still undergoing further follow-up, therefore, the prognosis of MVI-positive grading patients has not been studied. In the future, efforts will be made to expand the sample size, incorporate external validation data to ensure the generalizability of the model; meanwhile, the prognosis of included patients will be followed up to study early postoperative recurrence, overall survival time, and time to recurrence.

Conclusion

In conclusion, MRI radiomics models based on intra-tumoral and peri-tumoral features can effectively predict MVI grading in hepatocellular carcinoma (≤3 cm). The combination of intra-tumoral and peri-tumoral features outperformed the intra-tumoral model alone, with the $AVDP_{intra+peri3mm}$ model yielding the best predictive performance. Moreover, the CRR model demonstrated the optimal predictive performance.

Data Sharing Statement

The original contributions presented in the study are included in the article/Supplementary Material. Further inquiries can be directed to the corresponding authors.

Author Contributions

All authors made a significant contribution to the work reported, whether that is in the conception, study design, execution, acquisition of data, analysis and interpretation, or in all these areas; took part in drafting, revising or critically reviewing the article; gave final approval of the version to be published; have agreed on the journal to which the article has been submitted; and agree to be accountable for all aspects of the work.

Funding

This research was supported by Shanghai Municipal Health Commission (2022LJ024).

Disclosure

The authors report no conflicts of interest in this work.

References

1. Jemal A, Bray F, Center MM, Ferlay J, Ward E, Forman D. Global cancer statistics. *Ca a Cancer J Clinicians*. 2011;61(2):69–90. doi:10.3322/caac.20107
2. Villanueva A. Hepatocellular Carcinoma. *New Engl J Med*. 2019;380(15):1450–1462. doi:10.1056/NEJMra1713263
3. Tabrizian P, Jibara G, Shrager B, Schwartz M, Roayaie S. Recurrence of hepatocellular cancer after resection: patterns, treatments, and prognosis. *Ann Surg*. 2015;261(5):947–955. doi:10.1097/SLA.0000000000000710
4. Bruix J, Gores GJ, Mazzaferro V. Hepatocellular carcinoma: clinical frontiers and perspectives. *Gut*. 2014;63(5):844–855. doi:10.1136/gutjnl-2013-306627
5. Cong WM, Wu MC. Small hepatocellular carcinoma: current and future approaches. *Hepatol Internat*. 2013;7(3):805–812. doi:10.1007/s12072-013-9454-z
6. Cong WM, Bu H, Chen J, et al. Practice guidelines for the pathological diagnosis of primary liver cancer: 2015 update. *World J Gastroenterol*. 2016;22(42):9279–9287. doi:10.3748/wjg.v22.i42.9279
7. Rodríguez-Perálvarez M, Luong TV, Andreana L, Meyer T, Dhillon AP, Burroughs AK. A systematic review of microvascular invasion in hepatocellular carcinoma: diagnostic and prognostic variability. *Ann Surg Oncol*. 2013;20(1):325–339. doi:10.1245/s10434-012-2513-1
8. Lee S, Kim SH, Lee JE, Sinn DH, Park CK. Preoperative gadoxetic acid–enhanced MRI for predicting microvascular invasion in patients with single hepatocellular carcinoma. *J Hepatol*. 2017;67(3):526–534. doi:10.1016/j.jhep.2017.04.024
9. Zhou JM, Zhou CY, Chen XP, Zhang ZW. Anatomic resection improved the long-term outcome of hepatocellular carcinoma patients with microvascular invasion: a prospective cohort study. *World J Gastrointest Oncol*. 2021;13(12):2190–2202. doi:10.4251/wjgo.v13.i12.2190
10. Sumie S, Nakashima O, Okuda K, et al. The significance of classifying microvascular invasion in patients with hepatocellular carcinoma. *Ann Surg Oncol*. 2014;21(3):1002–1009. doi:10.1245/s10434-013-3376-9
11. Banerjee S, Wang DS, Kim HJ, et al. A computed tomography radiogenomic biomarker predicts microvascular invasion and clinical outcomes in hepatocellular carcinoma. *Hepatology*. 2015;62(3):792–800. doi:10.1002/hep.27877
12. Dhir M, Melin AA, Douaiher J, et al. A Review and Update of Treatment Options and Controversies in the Management of Hepatocellular Carcinoma. *Ann Surg*. 2016;263(6):1112–1125. doi:10.1097/SLA.0000000000001556
13. Yang S, Ni H, Zhang A, Zhang J, Zang H, Ming Z. Significance of anatomical resection and wide surgical margin for HCC patients with MVI undergoing laparoscopic hepatectomy: a multicenter study. *Eur J Surg Oncol*. 2025;51(1):109353. doi:10.1016/j.ejso.2024.109353
14. Renzulli M, Brocchi S, Cucchetti A, et al. Can Current Preoperative Imaging Be Used to Detect Microvascular Invasion of Hepatocellular Carcinoma? *Radiology*. 2016;279(2):432–442. doi:10.1148/radiol.2015150998
15. Sasaki M, Yamada K, Watanabe Y, et al. Variability in absolute apparent diffusion coefficient values across different platforms may be substantial: a multivendor, multi-institutional comparison study. *Radiology*. 2008;249(2):624–630. doi:10.1148/radiol.2492071681
16. Bharti P, Mittal D, Ananthasivan R. Preliminary Study of Chronic Liver Classification on Ultrasound Images Using an Ensemble Model. *Ultrasonic Imag*. 2018;40(6):357–379. doi:10.1177/0161734618787447
17. Wang H, Feng LH, Qian YW, Cao ZY, Wu MC, Cong WM. Does microvascular invasion in Barcelona Clinic Liver Cancer stage A multinodular hepatocellular carcinoma indicate early-stage behavior? *Ann translat Med*. 2019;7(18):428. doi:10.21037/atm.2019.08.114
18. Nebbia G, Zhang Q, Arefan D, Zhao X, Wu S. Pre-operative Microvascular Invasion Prediction Using Multi-parametric Liver MRI Radiomics. *J Digital Imaging*. 2020;33(6):1376–1386. doi:10.1007/s10278-020-00353-x
19. Tian Y, Hua H, Peng Q, et al. Preoperative Evaluation of Gd-EOB-DTPA-Enhanced MRI Radiomics-Based Nomogram in Small Solitary Hepatocellular Carcinoma (≤3 cm) With Microvascular Invasion: a Two-Center Study. *J Magn Reson Imaging*. 2022;56(5):1459–1472. doi:10.1002/jmri.28157
20. Liu HF, Wang M, Wang Q, et al. Multiparametric MRI-based intratumoral and peritumoral radiomics for predicting the pathological differentiation of hepatocellular carcinoma. *Insights Imaging*. 2024;15(1):97. doi:10.1186/s13244-024-01623-w
21. Roayaie S, Blume IN, Thung SN, et al. A system of classifying microvascular invasion to predict outcome after resection in patients with hepatocellular carcinoma. *Gastroenterology*. 2009;137(3):850–855. doi:10.1053/j.gastro.2009.06.003
22. Chernyak V, Fowler KJ, Kamaya A, et al. Liver Imaging Reporting and Data System (LI-RADS) Version 2018: imaging of Hepatocellular Carcinoma in At-Risk Patients. *Radiology*. 2018;289(3):816–830. doi:10.1148/radiol.2018181494
23. Imai K, Yamashita YI, Yusa T, et al. Microvascular Invasion in Small-sized Hepatocellular Carcinoma: significance for Outcomes Following Hepatectomy and Radiofrequency Ablation. *Anticancer Res*. 2018;38(2):1053–1060. doi:10.21873/anticanres.12322

24. Yamashita YI, Imai K, Yusa T, et al. Microvascular invasion of single small hepatocellular carcinoma ≤3 cm: predictors and optimal treatments. *Ann Gastroenterol Surg*. 2018;2(3):197–203. doi:10.1002/ags3.12057
25. Liu H, Yang Y, Chen C, et al. Reclassification of tumor size for solitary HBV-related hepatocellular carcinoma by minimum p value method: a large retrospective study. *World J Surg Oncol*. 2020;18(1):185. doi:10.1186/s12957-020-01963-z
26. Masuda T, Beppu T, Okabe H, et al. Predictive factors of pathological vascular invasion in hepatocellular carcinoma within 3 cm and three nodules without radiological vascular invasion. *Hepatol Res*. 2016;46(10):985–991. doi:10.1111/hepr.12637
27. Shindoh J, Kobayashi Y, Kawamura Y, et al. Microvascular Invasion and a Size Cutoff Value of 2 cm Predict Long-Term Oncological Outcome in Multiple Hepatocellular Carcinoma: reappraisal of the American Joint Committee on Cancer Staging System and Validation Using the Surveillance, Epidemiology, and End-Results Database. *Liver Cancer*. 2020;9(2):156–166. doi:10.1159/000504193
28. Lu XY, Xi T, Lau WY, et al. Hepatocellular carcinoma expressing cholangiocyte phenotype is a novel subtype with highly aggressive behavior. *Ann Surg Oncol*. 2011;18(8):2210–2217. doi:10.1245/s10434-011-1585-7
29. Lauwers GY, Terris B, Balis UJ, et al. Prognostic histologic indicators of curatively resected hepatocellular carcinomas: a multi-institutional analysis of 425 patients with definition of a histologic prognostic index. *Am J Surg Pathol*. 2002;26(1):25–34. doi:10.1097/00000478-200201000-00003
30. Hong SB, Choi SH, Kim SY, et al. MRI Features for Predicting Microvascular Invasion of Hepatocellular Carcinoma: a Systematic Review and Meta-Analysis. *Liver Cancer*. 2021;10(2):94–106. doi:10.1159/000513704
31. Yang WL, Zhu F, Chen WX. Texture analysis of contrast-enhanced magnetic resonance imaging predicts microvascular invasion in hepatocellular carcinoma. *Eur J Radiol*. 2022;156:110528. doi:10.1016/j.ejrad.2022.110528
32. Zheng X, Xu YJ, Huang J, Cai S, Wang W. Predictive value of radiomics analysis of enhanced CT for three-tiered microvascular invasion grading in hepatocellular carcinoma. *Med Phys*. 2023;50(10):6079–6095. doi:10.1002/mp.16597
33. Kow AW, Kwon CH, Song S, Shin M, Kim JM, Joh JW. Risk factors of peritoneal recurrence and outcome of resected peritoneal recurrence after liver resection in hepatocellular carcinoma: review of 1222 cases of hepatectomy in a tertiary institution. *Ann Surg Oncol*. 2012;19(7):2246–2255. doi:10.1245/s10434-012-2260-3
34. Chen ZH, Zhang XP, Feng JK, et al. Actual long-term survival in hepatocellular carcinoma patients with microvascular invasion: a multicenter study from China. *Hepatol Internat*. 2021;15(3):642–650. doi:10.1007/s12072-021-10174-x
35. Yang Y, Fan W, Gu T, et al. Radiomic Features of Multi-ROI and Multi-Phase MRI for the Prediction of Microvascular Invasion in Solitary Hepatocellular Carcinoma. *Front Oncol*. 2021;11:756216. doi:10.3389/fonc.2021.756216
36. Lu XY, Zhang JY, Zhang T, et al. Using pre-operative radiomics to predict microvascular invasion of hepatocellular carcinoma based on Gd-EOB-DTPA enhanced MRI. *BMC Med. Imaging*. 2022;22(1):157. doi:10.1186/s12880-022-00855-w
37. Feng S-T, Jia Y, Liao B, et al. Preoperative prediction of microvascular invasion in hepatocellular cancer: a radiomics model using Gd-EOB-DTPA-enhanced MRI. *Eur Radiol*. 2019;29(9):4648–4659. doi:10.1007/s00330-018-5935-8
38. Yu Y, Song J, Zhang R, et al. Preoperative neutrophil-to-lymphocyte ratio and tumor-related factors to predict microvascular invasion in patients with hepatocellular carcinoma. *Oncotarget*. 2017;8(45):79722–79730. doi:10.18632/oncotarget.19178
39. Fan Y, Mao R, Yang J. NF-κB and STAT3 signaling pathways collaboratively link inflammation to cancer. *Protein Cell*. 2013;4(3):176–185. doi:10.1007/s13238-013-2084-3